

where σ_n^μ are Pauli matrices and $h_n \in [-W, W]$ are independent uniformly distributed random variables. The Jordan-Wigner transformation maps this Hamiltonian exactly to non-interacting spinless fermions hopping on a disordered lattice [27], and a spin current in the XX model corresponds to a particle current in the fermionic language. The driving and dephasing are described by the Lindblad master equation:

$$\frac{d\rho}{dt} = i[\rho, \mathcal{H}] + \sum_{k=0}^{L+1} ([L_k \rho, L_k^+] + [L_k, \rho L_k^+]). \quad (2)$$

The spin current is driven by the jump operators:

$$L_0 = \sqrt{2\Gamma}\sigma_1^+ \quad L_{L+1} = \sqrt{2\Gamma}\sigma_L^-, \quad (3)$$

and the onsite dephasing by the jump operators:

$$L_n = \sqrt{\gamma_n/2}\sigma_n^z \text{ for } n = 1, 2, \dots, L, \quad (4)$$

where for each site $\gamma_n = 0$ with probability p and $\gamma_n = \gamma$ with probability $1 - p$.

Similar setups have been used to study transport in both non-interacting [13, 28–30] and interacting [12, 13, 15, 16, 31, 32] quantum systems. After solving the Lindblad equation to find the non-equilibrium steady state (NESS) for a given realization of the disorder and dephasing, one can calculate the spin current j_∞ and in turn the resistance $R \propto 1/j_\infty$. The spin current from site n to site $n + 1$ is given by the expectation value of the operator $j_n = 2(\sigma_n^x \sigma_{n+1}^y - \sigma_n^y \sigma_{n+1}^x)$, as defined by the continuity equation for the local magnetization, and is independent of n in the NESS. The nature of the transport can then be determined by the scaling of the typical resistance with the system size, $R \propto L^\beta$, where $\beta = 1$ indicates diffusion and $\beta > 1$ indicates subdiffusion (localization is signalled by $R \propto \exp(L/\xi)$, with ξ the localization length, implying a divergence of β). Similarly, as discussed earlier, the distribution of resistances can reveal the mechanism for subdiffusion, with the Griffiths effects picture necessarily implying the existence of heavy-tailed distributions.

The advantage of studying this non-interacting model is that the NESS current can be found exactly by manipulating matrices with dimensions equal to the system size L , rather than 4^L as would be the case with the full many-body state space. This allows for the efficient numerical solution of large systems with $L \sim 1000$, without the need for approximations based on matrix-product operator methods [28, 29, 33]. Details of the numerical method can be found in Appendix A. These large system sizes are essential when studying transport and localization phenomena in disordered quantum systems due to strong finite-size effects [12, 34–36].

In the limit of no dephasing, $p = 1$, the system is Anderson localized (i.e. an insulator), and the resistance grows with system size as $R \propto e^{L/\xi}$ [1, 13, 29]. In the opposite limit with dephasing on every site, $p = 0$, the system is a diffusive conductor with $R \propto L$ [28, 29]. For intermediate p , the system is made up of a series

of these insulating and conducting regions, and as p becomes large there will be an increasing number of long insulating segments. This results in regions of the system with exponentially large resistances, and one might therefore expect subdiffusive transport as described by the Griffiths effects picture. We explore this argument more thoroughly in Section III.

In our numerical study we use the parameters $\Gamma = 1$ and $\gamma = 0.2$, and for a fixed disorder strength $W = 1, 2, 3, 4$ we vary the dephasing fraction p to probe the different regimes of transport. For each parameter combination we sample many realizations of the disorder and dephasing (a minimum of 5000 for $L < 256$, 500 for $L \geq 256$, and 200 for $L = 1024$), and we ensure that at least 95% of the realizations converge to the correct NESS. We perform numerical fits to the median resistance $R_\star(L)$ to determine the asymptotic scaling exponent β , including finite-size corrections. We find that different finite-size corrections match the data more accurately in different parameter regimes. Defining $x = \ln L$ and $y = \ln R_\star$, we use a fit of the form $y = a + \beta x + b/x$ for $W \geq 2$ and $R_\star = a(1 + b/L)L^\beta$ for $W = 1$ (in both cases these forms outperform a simple fit to $R_\star = aL^\beta$ with the smallest system sizes omitted). Applying different fits can change the values of β and the location of a potential transition to subdiffusion.

A. Finite-size effects: Three lengths

As described above, the behavior of the finite-size corrections are markedly different for $W = 1$ and $W = 4$, and different fitting functions work better for $R_\star(L)$. This is evident in Fig. 1: the upper panel shows the scaling of the resistance with system size for a system with dephasing on every site, $p = 0$, where for $W = 1$ we see very similar behavior to that in the disorder-free case. In the absence of dephasing and disorder the system exhibits ballistic transport, and the diffusion in the clean system with dephasing is a result of scattering due to the dephasing. At stronger disorder (see Ref. 29) we see a change of behavior, with R approaching the asymptotic diffusive behavior from below, initially increasing faster than linearly with L . Our task is now to introduce length and resistance scales which separate the different behaviors. These different flows with L are caused by the interplay of three length scales: a length associated with dephasing strength γ (which we will call ℓ), one with disorder W (the localization length ξ), and the third with the density of dephasing sites p (the largest cluster of sites without dephasing s_\star).

First, we will consider the largest “insulator” size s_\star , which depends only on the density of dephasing sites p . From percolation theory in one dimension it is known that the typical value of the largest cluster of sites with *no dephasing* is $s_\star = \log_{1/p}(L[1 - p])$, to lowest order in $1/L$ [37]. For the Griffiths picture to apply the resistance of these rare clusters must be exponentially large in s_\star

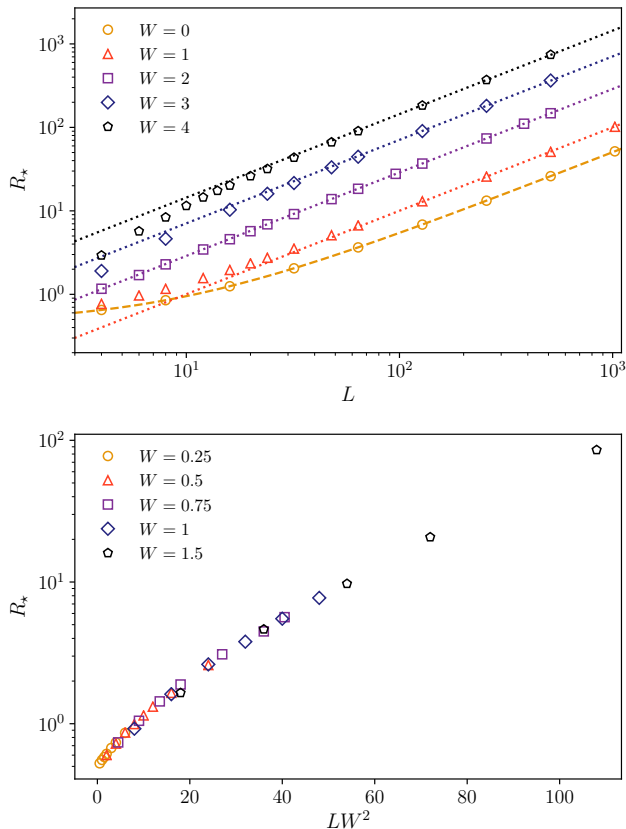


Figure 1. Finite-size effects in the resistance scaling. Upper panel: Median resistance R_* as a function of system size L for several disorder strengths W in a system with dephasing on every site ($p = 0$). Dotted lines indicate the asymptotic diffusive scaling and the dashed line shows the exact result in the absence of disorder. Lower panel: Median resistance R_* as a function of the rescaled length LW^2 for several disorder strengths W in a system with no dephasing ($p = 1$), showing the scaling of the localization length at weak disorder $\xi \propto W^{-2}$.

to create the power-law tail of $P(R)$. Therefore, one needs $s_* \gg \xi$ so that the cluster is truly localized. If this condition is satisfied, then the contribution to the resistance of the largest cluster is indeed $R_* \propto e^{s_*/\xi} = L^\beta$ with $\beta = 1/(\xi \ln(1/p))$.

The localization length in 1d (our second length-scale) is known to be $\xi = \frac{24}{W^2}$ [38, 39]. This is also shown in Figure 1 lower panel, where for $LW^2 \gtrsim 24$ the behavior of R is indeed exponential, while for $LW^2 \lesssim 24$ the behavior is power-law, $R \sim L^\beta$ with $\beta \sim 0.12$. Notice that the law $\xi \sim 24/W^2$ is only valid for $W \lesssim 2$, while for large W it is substituted by $\xi \sim 1/\ln W$ [40].

The condition that the largest cluster is localized reads:

$$\log_{1/p}(L[1-p]) \gg \frac{24}{W^2}. \quad (5)$$

To see that this is not always satisfied in our numerics, consider the parameter combination $p = 0.8, W = 1, L =$

1024: in this case $\xi = 24$ and (the average) $s_* = 25$, so the largest cluster is about one localization length. The second largest cluster is on average 21 lattice sites, so it is even smaller than a single localization length. Moreover, the logarithmic dependence means that if we want more than one localization length we must change L enormously: let us say we require

$$\log_{1/p}(L[1-p]) > c \frac{24}{W^2} \quad (6)$$

with a minimum confidence of, say, $c = 3$ (i.e. the largest cluster is at least 3 localization lengths). We see that

$$L > \frac{1}{1-p} \left(\frac{1}{p} \right)^{72/W^2}, \quad (7)$$

and, for $p = 0.8, W = 1$ as before, this condition implies $L > 10^7$. For $W = 3$, on the contrary, for $p = 0.5$ we get $L > 500$, which is still within our reach. We therefore conclude that, even for the values of $L = 10^3$ reached in our numerics, the data with $W = 1$ are deep in the pre-asymptotic regime, while for $W = 3, 4$ the data are representative of the asymptotic behavior (for p not too close to 1).

In a given realization of the system, if the longest string of sites without dephasing, s_0 , is larger than the localization length, $s_0 \gtrsim \xi$, then the distribution of the resistance has a heavy power-law tail. This can be seen by noting that the length of the longest insulating cluster s_0 obeys the Gumbel distribution for extreme values, with mode $s_* = \log_{1/p}(L[1-p])$ and standard deviation $\pi/(\sqrt{6} \ln(1/p))$ [37]. The cumulative distribution function of this length is then given by

$$F_{s_0}(s) = \exp(-\exp[(s_* - s) \ln(1/p)]). \quad (8)$$

Assuming that the resistance is dominated by this single long insulating cluster, and writing $q = e^{1/\xi}$, we have $R = R_1 q^{s_0}$. The distribution of the resistance is therefore:

$$P(R) = \exp\left(-L[1-p] \left[\frac{R_1}{R}\right]^{1/\beta}\right) \frac{L(1-p)R_1^{1/\beta}}{\beta R^{1+1/\beta}}, \quad (9)$$

where $\beta = \log_{1/p}(q)$ is the resistance scaling exponent. For $R \gg R_1$, this distribution decays with a tail $P(R) \propto R^{-1-1/\beta}$, exactly as the Griffiths picture would predict for the subdiffusive scaling $R \propto L^\beta$. If $\beta \leq 1$ then this argument does not hold, as the total resistance is not dominated by the longest insulating cluster.

However, if $s_0 \lesssim \xi$, then we are in the small LW^2 region in the lower panel of Fig. 1 (say $s_0 W^2 < 24$). As discussed above, in this region the law $R = q^s$ is not valid: it is replaced by a law of the form $R \sim s^\beta$ where, as said before, from the numerics $\beta \simeq 0.12$ (or at least $\beta \ll 1$). Using this relationship between s and R we find that the distribution of R decays like a stretched exponential

$$P(R) \sim e^{-cR^{1/\beta}}, \quad (10)$$

faster than a power law. We will observe exactly this in the numerics discussed in Section II B.

The third length, ℓ , is associated with a string of consecutive sites with dephasing. We study this case in more detail and present numerics in Fig. 1. We know that if dephasing is applied to every site of the chain, asymptotically one finds a resistance $R \propto L$. To a first approximation, if ξ is large we can consider the situation in the absence of disorder. In this case the resistance of a chain of length L with dephasing on every site has been calculated exactly in Ref. 28:

$$R = \frac{\gamma}{4} \left(1 + \frac{\Gamma + \Gamma^{-1} - \gamma}{\gamma L} \right) L, \quad (11)$$

which defines the asymptotic resistivity $\rho = \gamma/4$, or analogously the diffusion coefficient $D \propto 1/\gamma$. From the relation $D = v\ell$, where v is the velocity of excitations of the clean system (independent of γ), we see that $\ell \propto 1/\gamma$. The same length dominates the finite-size effects for $\gamma \ll \Gamma$ ($\Gamma = 1$ in our numerics) since we can write $R = \rho L (1 + 2\frac{\ell}{L})$.

For system sizes smaller than ℓ , or resistances smaller than $R_0 \equiv \rho\ell = \gamma\ell/4$, the resistance grows *slower* than L^1 , since the system goes from ballistic to diffusive transport. This can be seen by looking at the resistance beta function:

$$\frac{\partial \ln R}{\partial \ln L} = 1 - \frac{R_0}{R}. \quad (12)$$

On the other hand, if the disorder is much larger than the dephasing, $\xi \ll \ell$, for the systems with size L such that $\xi < L \ll \ell$ the resistance will scale exponentially with L . So, writing $R/R_1 = e^{L/\xi}$, in this regime:

$$\frac{\partial \ln R}{\partial \ln L} = \ln(R/R_1) > 1. \quad (13)$$

For $L > \ell$, however, it must reach the condition $\frac{\partial \ln R}{\partial \ln L} \rightarrow 1$.

Putting everything together we see that we can distinguish two regimes, depending on whether we have $\xi \lesssim L \ll \ell$ or $\ell \ll L \lesssim \xi$ (or in terms of resistances, whether we have $R_0 \ll R_1$ or $R_1 \ll R_0$). Fixing γ , we have large-disorder and small-disorder finite-size scaling behaviors which are completely different. We find, however, that an extremely good, phenomenological, two-parameter fit function is given by

$$\frac{\partial \ln R}{\partial \ln L} = 1 + \frac{\ln(R/R_a)}{1 + R/R_b}, \quad (14)$$

where $R_{a,b}$ are two fitting parameters. This form fits all data we have for any L, W, γ with good accuracy. The weak disorder case is obtained by $\ln(R_a/R^*)R_b = -R_0$ (for some R^* of the size of the observed resistances) while the large disorder case comes from the region $R \sim R_a = R_1 \ll R_b$. Fig. 2 shows examples of the beta function from our numerical data (calculated using a discrete derivative), showing good agreement with

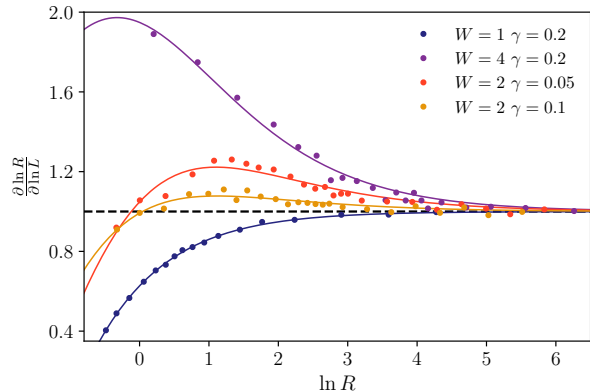


Figure 2. Resistance beta function for various disorder and dephasing values with $p = 0$ (discrete derivatives of the data in Fig. 1). We go from $W = 4, \gamma = 0.2$ which is large disorder and small dephasing to $W = 1, \gamma = 0.2$ which is small disorder. Intermediate cases $W = 2, \gamma = 0.05, 0.1$ are shown. Numerical results are fitted with a phenomenological function of the form (14), indicated by the lines of the corresponding color.

the phenomenological form (14) in the strong disorder, strong dephasing, and intermediate regimes.

We notice that this beta function is the same (except for an overall sign and the identification $g \propto 1/R$) as the typical conductance beta function which is amply described in the literature on disordered systems [41]. It can be computed in perturbation theory in the weak localization regime and in the strongly localized regime for a variety of cases. However, in the literature we have not found a discussion of this function in the setup of open system dynamics as presented above.

We are now ready to discuss the general scenario, with both random dephasing and disorder.

B. Results

Fig. 3 summarizes the behavior of the resistance for a system with $W = 3$. The lower panel shows an example of the power-law scaling of the median resistance R_* with system size for several dephasing fractions p ; the statistical uncertainties are smaller than the symbols and have therefore been omitted. It is clear that for $p \lesssim 0.4$ the lines are parallel, indicating the same scaling with L (we will show later that this corresponds to the diffusive phase), whereas for larger p the resistance grows more steeply with an exponent that increases with p . The black dashed line indicates the diffusive behavior $R_* \propto L$. We perform numerical fits to these data to determine the resistance scaling exponent β , including finite-size corrections as described above, which are indicated by the lines.

Histograms of the resistance for various parameter combinations are shown in the upper panels of Fig. 3.

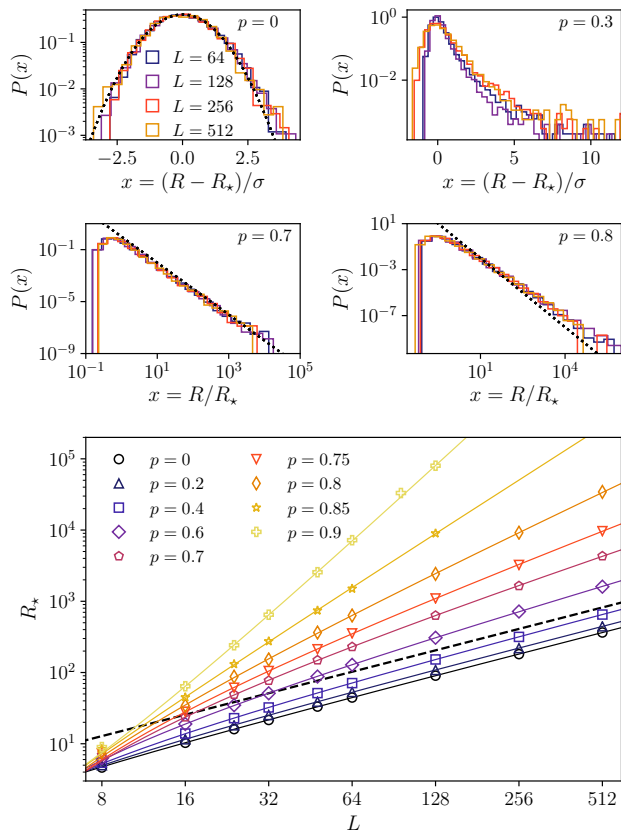


Figure 3. Numerical results on the resistance in the random dephasing model with $W = 3$. Upper panels: Histograms of the rescaled resistance in the diffusive phase $p = 0$ (top left) and $p = 0.3$ (top right), and the subdiffusive phase $p = 0.7$ (middle left) and $p = 0.8$ (middle right). The diffusive rescaling $(R - R_*)/\sigma$ is compared to a Gaussian distribution (black dotted line) for $p = 0$. In the subdiffusive phase the resistance is rescaled as R/R_* , and the black dotted lines indicate a R^{-2} tail. Lower panel: Scaling of the median resistance R_* with system size L for several dephasing fractions p . The lines in the corresponding color indicate the numerical fits to the data described in the text. The black dashed line indicates diffusive scaling $R_* \propto L$.

We find that, in the diffusive phase, the resistance distributions $P(R)$ for different system sizes can be collapsed by a rescaling $(R - R_*)/\sigma$, where $R_* \propto L$ is the average or typical value and $\sigma \propto \sqrt{L}$ is the standard deviation or width. Contrastingly, in the subdiffusive phase the collapse can be achieved by a rescaling of the form R/R_* , indicating that both the typical value and the width of the distribution grow like L^β . Deep in the diffusive phase the distribution is well approximated by a Gaussian (see the black dotted line on the $p = 0$ histogram), but as the system approaches the transition to subdiffusion a tail develops at large R (see the $p = 0.3$ histogram). In the subdiffusive phase we see heavy power-law tails in $P(R)$, as shown in the $p = 0.7$ and $p = 0.8$ histograms (the black dotted lines indicate the $P(R) \propto R^{-2}$ tail that

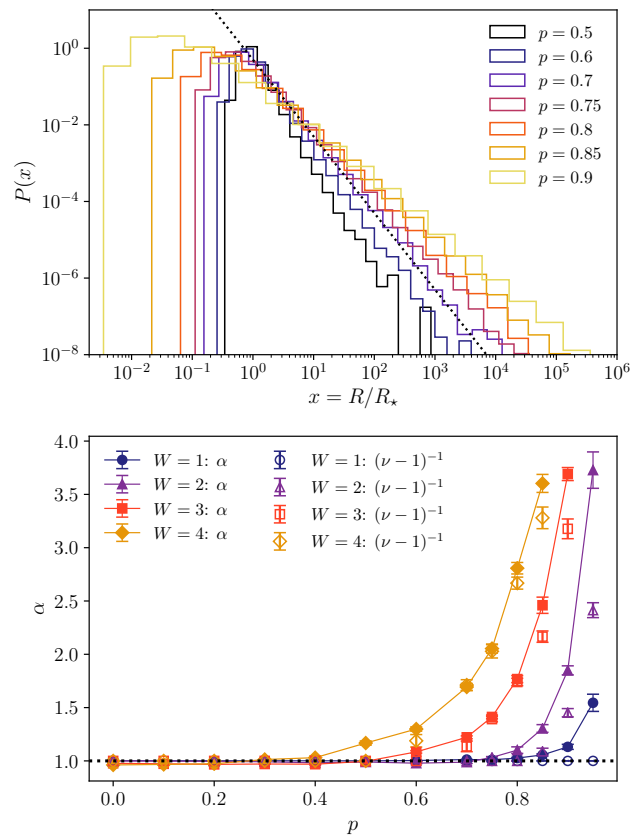


Figure 4. Upper panel: Histograms of the rescaled resistance R/R_* for $W = 3$, $L = 128$, and several dephasing fractions p . The black dotted line indicates a heavy R^{-2} tail. Lower panel: Comparison of the resistance scaling exponent β (connected filled points) with the predicted value based on the power-law tail of the histogram $(\nu - 1)^{-1}$ (unconnected unfilled points in the corresponding color). The discrepancy at $p \gtrsim 0.6$ and disorder $W \lesssim 3$ is attributed to the fact that the largest insulating cluster has a size s_* which is smaller than the localization length ξ , therefore the distribution of resistance does not show the appropriate power-law tail.

signals the onset of subdiffusion).

In the lower panel of Fig. 4 the connected filled points show the scaling exponent β , found from a fit to the median resistance value, as a function of the dephasing fraction p for several disorder strengths W . For each W the transport is diffusive for small p (i.e. $\beta = 1$), but upon increasing p above a critical value $p_c(W)$ the transport becomes subdiffusive (i.e. $\beta > 1$). The critical dephasing fraction $p_c(W)$ decreases with W , as the closed system is more strongly localized, and therefore the transport is weaker for a given p .

The upper panel of Fig. 4 shows histograms of R/R_* for a range of p values with $L = 128$ and $W = 3$, and the black dashed line shows the R^{-2} tail that signifies the onset of subdiffusion in the Griffiths effects picture. We see that in the subdiffusive phase ($p \gtrsim 0.5$) the distribution tails decay more slowly than R^{-2} and becomes

heavier as the transport becomes slower.

If the Griffiths effects picture is correct, the exponent of the histogram decay ν should be related to the exponent of the resistance scaling as $\beta = (\nu - 1)^{-1}$. The values of $(\nu - 1)^{-1}$ from the $L = 128$ histograms are shown by the unfilled points in the lower panel. We see that in the subdiffusive phase there is reasonable agreement for $W = 3$ and 4 when p is not too large, as discussed in Section II A, while for weaker disorder and large p the agreement becomes poor. The agreement is also poor close to the transition point, where the histogram tails would suggest weaker subdiffusion than the resistance scaling.

III. Exactly solvable semiclassical model

In order to understand the results shown in the previous section, we now examine a related phenomenological semiclassical model. Consider a chain of L units, where each unit may be either an insulator with probability p , or a conductor with probability $1 - p$. Conductors combine linearly, with each conductor contributing a resistance of R_0 , so a string of conductors of length s has a resistance of $R_0 s$. Because of phase coherence, insulators combine multiplicatively, so a string of insulators of length s has a resistance of $R_1 q^s$, where $q > 1$. The total resistance of the chain is then equal to

$$R = R_0 \sum_{s \geq 1} n_c(s) s + R_1 \sum_{s \geq 1} n_i(s) q^s, \quad (15)$$

where $n_c(s)$ ($n_i(s)$) is the number of strings of conductors (insulators) of length s . The relationship with the microscopic dephasing model is as follows: strings of sites without dephasing are modelled by strings of insulators (a shorter localization length due to stronger disorder corresponds to a larger q), and strings of sites with dephasing are modelled by strings of conductors.

A. Analytical results

We will now analyse the statistical properties of the total resistance R . In order to determine the average resistance across configurations, we note that the quantities $n_c(s)$ and $n_i(s)$ are Poisson-distributed random variables:

$$P(n(s)) = \frac{\mu(s)^{n(s)}}{n(s)!} e^{-\mu(s)}, \quad (16)$$

where $\mu = \langle n(s) \rangle$, with the angled brackets denoting an average over different configurations of conductors and insulators. This is subject to the constraint:

$$\sum_{s \geq 1} s n_c(s) + \sum_{s \geq 1} s n_i(s) = L. \quad (17)$$

The mean values are

$$\begin{aligned} \mu_c(s) &= \langle n_c(s) \rangle = L p^2 (1 - p)^s, \\ \mu_i(s) &= \langle n_i(s) \rangle = L (1 - p)^2 p^s. \end{aligned} \quad (18)$$

The constraint (17) is then satisfied on average for $L \gg 1$:

$$\sum_{s \geq 1} \langle s n_c(s) + s n_i(s) \rangle = L p + L (1 - p) L = L. \quad (19)$$

The average resistance is therefore given by

$$\langle R \rangle = L R_0 (1 - p) + L R_1 \sum_{s \geq 1} (1 - p)^2 (q p)^s. \quad (20)$$

When $p q < 1$ the sum (20) converges, and the average total resistance grows linearly with system size, meaning the system is diffusive:

$$\begin{aligned} \langle R \rangle &= R_0 (1 - p) L + R_1 \frac{p q (1 - p)^2}{1 - p q} L \\ &= R'_0 L. \end{aligned} \quad (21)$$

On the other hand, for $p q \geq 1$, the sum (20) does not converge and the average does not exist. In this regime, the total resistance for a given configuration is dominated by the longest string of consecutive insulators, which has a typical length of $s_* \approx \log_{1/p}(L[1 - p]) \approx \log_{1/p}(L)$ for large L [37]. This then results in a typical resistance of

$$R \sim R_1 q^{\log_{1/p}(L)} \propto L^{\log_{1/p}(q)}, \quad (22)$$

resulting in the subdiffusive scaling exponent $\beta = \log_{1/p}(q)$. The system therefore has a transition from a diffusive phase to a subdiffusive phase at $p_c = 1/q$. In this phase we expect the total resistance to be distributed according to (9), as the arguments leading to this expression are identical to those described above. Therefore we expect the subdiffusive phase to be described by the physics of Griffiths effects, with heavy-tailed resistance distributions: $P(R) \propto R^{-1-1/\beta}$ (note that in this phenomenological model the resistances of the insulating clusters are always exponential in their size, so the finite-size effects leading to (10) do not apply).

We now examine the properties of the distributions of R more carefully and show that this is true. The Laplace transform of the distribution of the insulating part of the resistance $R_i = \sum_{s=1}^L n_i(s) q^s$ (i.e. its moment generating function) is equal to:

$$\begin{aligned} \langle e^{-\rho R_i} \rangle &= \prod_{s=1}^L \langle e^{-\rho n_i(s) q^s} \rangle \\ &= \prod_{s=1}^L \exp\left(-\mu_s + \mu_s e^{-\rho q^s}\right) \\ &\equiv e^{-\phi(\rho)}, \end{aligned} \quad (23)$$

where the second line follows from evaluating the average for the single $n_i(s)$ with $L \rightarrow \infty$. The cumulant generating function for R_i is therefore given by $\phi(\rho) = \sum_{s=1}^L \mu_s (1 - e^{-\rho q^s})$. Examining the lowest few cumulants we find:

$$\begin{aligned}\phi(0) &= 0 \\ \langle R_i \rangle &= \phi'(0) = \sum_{s=1}^L \mu_s q^s = L(1-p)^2 \sum_{s=1}^L (pq)^s \\ \langle \delta R_i^2 \rangle &= -\phi''(0) = \sum_{s=1}^L \mu_s q^{2s} = L(1-p)^2 \sum_{s=1}^L (pq^2)^s \\ \langle \delta R_i^3 \rangle &= \phi'''(0) = \sum_{s=1}^L \mu_s q^{3s} = L(1-p)^2 \sum_{s=1}^L (pq^3)^s\end{aligned}\quad (24)$$

where $\delta R_i = R_i - \langle R_i \rangle$. If each sum converged as $L \rightarrow \infty$, then the distribution would have a limit where every cumulant is proportional to L . However, for $q > 1$ and any $p > 0$ there always exists an n such that $pq^n > 1$. Defining $\tau = \log_{1/p}(q)$, the smallest integer larger than $1/\tau$ corresponds to the lowest cumulant that scales superlinearly with L , and all subsequent moments will scale with a different power of L (note that $\beta = \tau$ in the subdiffusive phase). In other words, when $p > q^{-n}$ the n^{th} cumulant stops growing linearly with L , and begins to scale like $L^{n\tau}$.

To analyse the distribution of R_i , we extend the sum to $L \rightarrow \infty$, therefore neglecting terms exponentially small in L :

$$\begin{aligned}\phi(\rho) &= \sum_{s=1}^{\infty} \mu_s - L(1-p)^2 \sum_{s=1}^{\infty} p^s e^{-\rho q^s} \\ &= L(1-p) - L(1-p)^2 \psi(\rho),\end{aligned}\quad (25)$$

where

$$\psi(\rho) \equiv \sum_{s=1}^{\infty} p^s e^{-\rho q^s}.\quad (26)$$

We evaluate the sum after taking the Mellin transform:

$$\begin{aligned}M(z) &= \int_0^{\infty} d\rho \rho^{z-1} \psi(\rho) = \sum_{s=1}^{\infty} p^s \Gamma(z) q^{-sz} \\ &= \Gamma(z) \frac{1}{p^{-1}q^z - 1},\end{aligned}\quad (27)$$

where $\Gamma(z)$ is the gamma function. The inverse transform therefore gives

$$\psi(\rho) = \int_{c-i\infty}^{c+i\infty} \frac{dz}{2\pi i} \rho^{-z} \Gamma(z) \frac{1}{p^{-1}q^z - 1},\quad (28)$$

where the integration path is the Bromwich contour \mathcal{B} shown in the left panel of Fig. 5. The expansion for small ρ can be obtained by moving the contour of the z -integration to the left (see the right panel of Fig. 5),

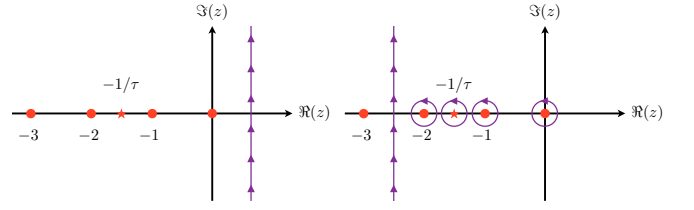


Figure 5. The contours used to evaluate the integral in (28) for small ρ . Poles of the integrand are indicated in red (poles of the Gamma function as circles and the other pole as a star) and the integration contour is indicated in purple. Left: The Bromwich contour used in (28). Right: Deformation of the contour by pushing it to the left, picking up the leading orders in ρ as each pole is enclosed.

picking up the leading-order terms with each pole. The gamma function has simple poles on all the negative integers, with the pole at $-m$ giving a contribution of $\frac{(-\rho)^m}{m!(p^{-1}q^{-m}-1)}$ to the integral. There is another simple pole located at $z = -1/\tau < 0$, which gives a contribution of $\rho^{1/\tau} \Gamma(-1/\tau) \ln(q)$ (there is also a sequence of image poles at $z = -1/\tau + 2\pi i n / \ln(q)$ for $n \in \mathbb{Z}$, however, their contribution is strongly suppressed by their distance from the real line for reasonable values of $q \lesssim 10$).

The leading-order terms depend on the value of τ , resulting in several regimes. If $1/\tau > 2$ we find:

$$\begin{aligned}\phi(\rho) &= \frac{L(1-p)^2 pq}{1-pq} \rho - \frac{1}{2} \frac{L(1-p)^2 pq^2}{1-pq^2} \rho^2 + o(\rho^2) \\ &= \langle R_i \rangle \rho - \frac{1}{2} \langle \delta R_i^2 \rangle \rho^2 + o(\rho^2);\end{aligned}\quad (29)$$

stopping at quadratic order, we recognize the cumulant generating function of a Gaussian distribution:

$$P(R_i) = \int_{\mathcal{B}} \frac{d\rho}{2\pi i} e^{\rho R_i - \phi(\rho)} = \frac{1}{\sqrt{2\pi \langle \delta R_i^2 \rangle}} e^{-\frac{(R_i - \langle R_i \rangle)^2}{2\pi \langle \delta R_i^2 \rangle}}.\quad (30)$$

However, if $1 < 1/\tau < 2$ the pole at $z = -1/\tau$ contributes, giving:

$$\phi(\rho) = \langle R_i \rangle \rho - \frac{L(1-p)^2 \Gamma(-\tau^{-1})}{\ln(q)} \rho^{1/\tau} + o(\rho^{1/\tau}).\quad (31)$$

Stopping at this order, we recognize the result as consistent with a Lévy alpha-stable distribution with average $\langle R_i \rangle$, and a scale that grows as $\delta R_i^2 \propto L^{2\tau} \gg L$. The stability parameter is equal to $1/\tau$, resulting in a distribution with a tail decaying asymptotically as $P(R_i) \propto R_i^{-1-1/\tau}$. If $1/\tau < 1$ then the distribution has a heavy tail and the average no longer exists, so we must instead consider the typical value of R_i . Noting that in this regime $\beta = \tau$, we recognize the heavy-tailed distribution from the Griffiths effects argument, $P(R_i) \propto R_i^{-1-1/\beta}$, resulting in the scaling $R \approx R_i \propto L^\beta$.

B. Numerical results

We now study the system numerically in order to confirm the accuracy of the analysis above. The results shown correspond to the parameters: $R_0 = 1$, $R_1 = 1.5$, and $q = 1.5$. By changing p we can tune the system across the diffusion-subdiffusion transition, which should be found at $p_c = 2/3$. We introduce additional randomness by making $R_i(s)$ the product of s random variables q_n , each drawn independently from a narrow uniform distribution in the range $q \pm 0.1$, so $R_i(s) = R_1 \prod_{n=1}^s q_n$ (note that on average $R_i(s)$ is still equal to $R_1 q^s$); this has no effect on the results other than to smooth the histograms of R . The numerical analysis of this model requires no solution of matrix equations, unlike the microscopic model in Section II, allowing us to extensively sample very large system sizes: the results below include systems of up to $L = 6400$ and $\sim 10^5$ samples.

A comparison between the numerical results and the analytical predictions is shown in Fig. 6. The lower panel shows a good agreement between the resistance scaling exponent β , calculated using the median resistance R_* for $L \geq 800$, with the theoretical prediction: $\beta = 1$ for $p < p_c = 2/3$ and $\beta = \log_{1/p}(q)$ for $p > 2/3$. We also see that the width of the distributions, measured by the inter-quartile range (IQR), also scales as expected: for $\text{IQR} \propto L^{\beta'}$ we find $\beta' = 1/2$ for $p < q^{-2} = 4/9$ and $\beta' = \log_{1/p}(q)$ for $p > 4/9$. The predicted values for β and β' are indicated by the dashed and dotted black lines respectively (the line becomes dot-dashed for $p > p_c$, where $\beta = \beta'$). The upper panels show histograms of the resistance over a range of p values. Deep in the diffusive phase ($p = 0.1$ in the figure) the distribution is approximately Gaussian (indicated by the black dotted line), with the average and median growing linearly with L and the standard deviation growing like \sqrt{L} . Closer to the subdiffusion transition ($p = 0.3$ in the figure) the distribution starts to develop a tail (these parameters correspond to the point where the third cumulant has started to scale faster than linearly with L , $pq^3 = (0.3)(1.5)^3 = 81/80$). Close to the subdiffusion transition on the diffusive side ($p = 0.5$ in the figure), where the average is still defined but the variance is not, $pq^2 = (0.5)(1.5)^2 = 9/8$) we see that the distribution has developed the predicted weak power-law tail which is indicated by the black dotted line. In the subdiffusive phase ($p = 0.9$ in the figure) the distribution has a strong power-law tail, which agrees well with the prediction (9) that R is dominated by the longest string of insulators, shown again by the black dotted line. The discrepancy at small R is due to the fact that these realizations have unusually short longest strings of insulators, which therefore have a less dominant contribution to the total resistance.

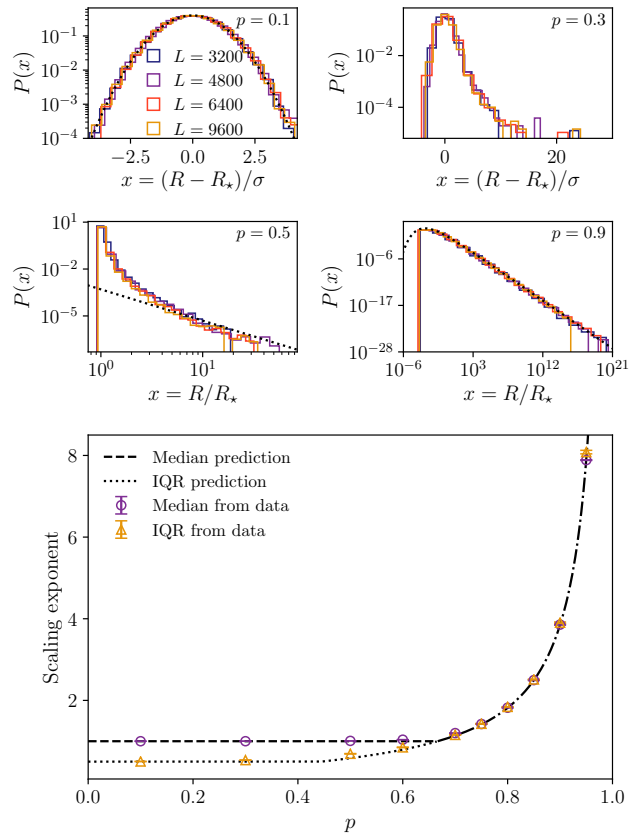


Figure 6. Comparison of analytical and numerical results for the semiclassical model. Upper panels: Histograms of the rescaled resistance in the diffusive phase $p = 0.1$ (top left), $p = 0.3$ (top right), and $p = 0.5$ (center left) and the subdiffusive phase $p = 0.9$ (center right). The top panels show the rescaling $(R - R_*)/\sigma$, which is compared to a Gaussian distribution (black dotted line) for $p = 0.1$, the existence of a tail in the diffusive phase is clear in the $p = 0.3$ histogram. The central panels show the rescaling R/R_* , with a comparison to the predicted tail for $p = 0.5$, and a comparison to the theoretical prediction (9) shown for $p = 0.9$ (black dotted lines). Lower panel: Comparison of the numerically determined scaling exponent for the median resistance, β , and also for the inter-quartile range, β' , with the analytical prediction $\log_{1/p}(q)$.

IV. Discussion

In this paper we have studied DC spin transport in a disordered, non-interacting spin chain with dephasing on random sites. We have shown that the system exhibits a phase transition from diffusive to subdiffusive transport when the density of sites with dephasing decreases below a critical value. In the subdiffusive phase the distributions of resistances across different realizations of the disorder and dephasing have heavy tails, suggesting that the subdiffusion is caused by Griffiths effects.

We have also presented a related, exactly solvable semiclassical model, where the system is formed of ran-

domly chosen sequences of insulators and conductors. We have shown that this system also undergoes a transition from diffusion to subdiffusion due to Griffiths effects when the density of conductors decreases below a critical value. This model captures the qualitative features seen in the microscopic quantum model, including the Gaussian distributions of resistances deep in the diffusive phase, which develop tails as the transition to subdiffusion is approached, and eventually become heavy-tailed in the subdiffusive phase.

The behavior of the quantum model is most similar to that of the semiclassical model (i.e. most consistent with the physics of Griffiths effects) when the disorder is strong and the subdiffusion weak. We have argued that this discrepancy is due to the finite lengths of the clusters of sites with and without dephasing: the semiclassical model is constructed using the asymptotic scaling properties of these clusters, and we have shown that for certain parameter combinations they are certainly not in their asymptotic regimes. At very large system sizes we expect that the behavior of the two models will become increasingly similar.

Studies on interacting disordered quantum systems have failed to find definitive evidence for Griffiths effects being the cause of subdiffusive transport. This may be due to strong finite-size effects, as it is known that large system sizes are required to observe the asymptotic transport properties in interacting systems [12]. In Ref. 13 it was shown that accurately simulating subdiffusive dynamics requires high bond dimensions in the time-evolving block decimation (TEBD) algorithm, so characterizing the subdiffusion in a large system has a restrictively high computational cost. These TEBD studies on subdiffusion in large systems [12, 13, 15, 16] are limited to $L \lesssim 100$ in the subdiffusive phase, with the maximum achievable L decreasing as the disorder strength increases and the transport becomes slower. Presumably in interacting systems, if the regions of strong disorder are not large enough to act as bottlenecks to transport, the nature of the subdiffusion may be concealed by finite-size effects similar to those described in Section II A: the subdiffusive scaling of R_* with L in the absence of heavy-tailed distributions, shown for $W = 1$ in Fig. 4, mirrors the results in Ref. 13.

We also observe similarities between the finite-size scaling of the resistance in the interacting system and in our dephasing model. The scaling properties of the NESS current with system size in the thermalizing phase of the disordered Heisenberg spin chain were first presented in Ref. 12, and we have reproduced the results in Fig. 7 (we maintain the convention from the original paper of stating disorder strength in relation to onsite fields that couple to spin operators, not Pauli matrices). In the original paper the authors examined the average current $\langle j \rangle$ rather than the resistance, but the quantity $\tilde{R} = 1/\langle j \rangle$ should behave in the same way as the typical (median) resistance, as the distribution of currents does not have a large tail. In the upper panel of Fig. 7 the points

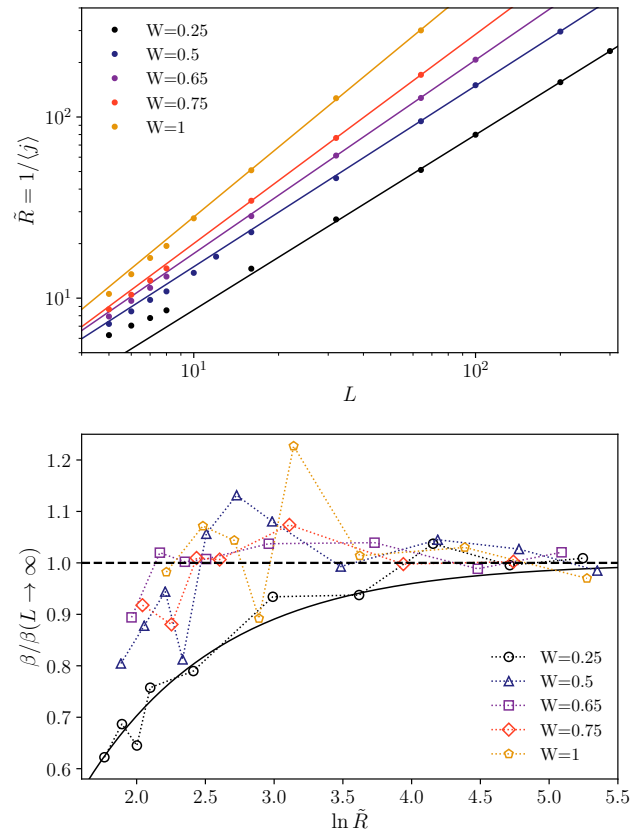


Figure 7. Scaling properties of the inverse NESS current with system size in the disordered Heisenberg spin chain. Upper panel: \tilde{R} as a function of L for several disorder strengths in the thermalizing phase. The points show the numerical data, and the lines indicate a fit of the form $\tilde{R} = aL^\beta$ using the three largest system sizes. Lower panel: The (discrete) beta function of the same data, normalized by its asymptotic value at $L \rightarrow \infty$. The solid black line indicates a fit of the form (12) to the $W = 0.25$ data. Data reproduced from Ref. 12.

show numerical data and the lines indicate fits of the form $\tilde{R} = aL^\beta$ evaluated on the largest three system sizes available. We see comparable behavior to that in Fig. 1: for weak disorder \tilde{R} approaches the asymptotic power-law scaling from above (note that the transport in the clean isotropic Heisenberg model is superdiffusive but not ballistic), while for stronger disorder it approaches the asymptotic scaling from below. In the lower panel of Fig. 7 we show the discrete resistance beta function, which we have normalised by its asymptotic value, β , to better compare the diffusive ($W \lesssim 0.55$) and subdiffusive ($W \gtrsim 0.55$) data. We see very similar behavior to that in Fig. 2: for weak disorder the beta function approaches its asymptotic value from below (a fit of the form (12) is shown for $W = 0.25$), while for stronger disorder the asymptotic behavior is approached from above. This suggests that the physics of the dephasing model, and therefore this work, is relevant to fully interacting,

disordered systems (which can eventually be many-body localized) with weak disorder.

Determining the size of the rare insulating regions in interacting models, and how their size affects their effectiveness as bottlenecks, would be an important step in confirming or refuting the Griffiths effects hypothesis, and this could potentially be achieved using probes of local thermal properties such as those employed in Refs. 42 and 43. It could also be enlightening for the theory of the transition, helping in supporting and discriminating between the various renormalization groups scenarios [44–49] which have been proposed and which lead to different

critical properties of the dynamical MBL transition.

Acknowledgments

The authors would like to thank Sarang Gopalakrishnan, Vadim Oganesyan, Vipin Kerala Varma, and Marko Žnidarič for insightful discussions and collaborations in the early stages of this project. This work was supported by the Trieste Institute for the Theory of Quantum Technologies.

-
- [1] P. Anderson, *Phys. Rev.* **109**, 1492 (1958).
- [2] F. Evers and A. D. Mirlin, *Rev. Mod. Phys.* **80**, 1355 (2008).
- [3] D. M. Basko, I. L. Aleiner, and B. L. Altshuler, *Ann. Phys.* **321**, 1126 (2006).
- [4] V. Oganesyan and D. A. Huse, *Phys. Rev. B* **75**, 155111 (2007).
- [5] A. Pal and D. Huse, *Phys. Rev. B* **82**, 174411 (2010).
- [6] A. De Luca and A. Scardicchio, *Europhys. Lett.* **101**, 37003 (2013).
- [7] R. Nandkishore and D. A. Huse, *Annu. Rev. Condens. Matter Phys.* **6**, 15 (2015).
- [8] D. A. Abanin and Z. Papić, *Annalen der Physik* **529**, 1700169 (2017).
- [9] J. Z. Imbrie, V. Ros, and A. Scardicchio, *Annalen der Physik* **529**, 1600278 (2017).
- [10] K. Agarwal, S. Gopalakrishnan, M. Knap, M. Müller, and E. Demler, *Phys. Rev. Lett.* **114**, 160401 (2015).
- [11] Y. Bar Lev, G. Cohen, and D. R. Reichman, *Phys. Rev. Lett.* **114**, 100601 (2015).
- [12] M. Žnidarič, A. Scardicchio, and V. K. Varma, *Phys. Rev. Lett.* **117**, 040601 (2016).
- [13] M. Schulz, S. R. Taylor, A. Scardicchio, and M. Žnidarič, *Journal of Statistical Mechanics: Theory and Experiment* **2020**, 023107 (2020).
- [14] V. K. Varma, A. Leroze, F. Pietracaprina, J. Goold, and A. Scardicchio, *J. Stat. Mech.: Theory Exp.* **2017**, 053101 (2017).
- [15] M. Schulz, S. R. Taylor, C. A. Hooley, and A. Scardicchio, *Phys. Rev. B* **98**, 180201 (2018).
- [16] J. J. Mendoza-Arenas, M. Žnidarič, V. K. Varma, J. Goold, S. R. Clark, and A. Scardicchio, *Phys. Rev. B* **99**, 094435 (2019).
- [17] D. J. Luitz, N. Laflorencie, and F. Alet, *Phys. Rev. B* **93**, 060201 (2016).
- [18] I. Khait, S. Gazit, N. Y. Yao, and A. Auerbach, *Phys. Rev. B* **93**, 224205 (2016).
- [19] D. J. Luitz and Y. Bar Lev, *Phys. Rev. Lett.* **117**, 170404 (2016).
- [20] S. Gopalakrishnan, K. R. Islam, and M. Knap, *Phys. Rev. Lett.* **119**, 046601 (2017).
- [21] D. J. Luitz, I. Khaymovich, and Y. B. Lev, arXiv preprint arXiv:1909.06380 (2019).
- [22] M. Rispoli, A. Lukin, R. Schittko, S. Kim, M. E. Tai, J. Léonard, and M. Greiner, *Nature* **573**, 385 (2019).
- [23] W. De Roeck, F. Huveneers, and S. Olla, *Journal of Statistical Physics*, 1 (2020).
- [24] D. J. Luitz and Y. B. Lev, *Annalen der Physik* **529**, 1600350 (2017).
- [25] S. Gopalakrishnan and S. Parameswaran, *Physics Reports* **862**, 1 (2020).
- [26] J. P. Hulin, J. P. Bouchaud, and A. Georges, *Journal of Physics A: Mathematical and General* **23**, 1085 (1990).
- [27] P. Jordan and E. Wigner, *Z. Phys.*, 631 (1928).
- [28] M. Žnidarič, *J. Stat. Mech.: Theory Exp.* **2010**, L05002 (2010).
- [29] M. Žnidarič and M. Horvat, *European Physical Journal B* **86** (2013).
- [30] V. K. Varma, C. De Mulatier, and M. Žnidarič, *Phys. Rev. E* **96**, 032130 (2017).
- [31] M. Žnidarič, *New Journal of Physics* **12**, 043001 (2010).
- [32] M. Žnidarič, *Journal of Statistical Mechanics: Theory and Experiment* **2011**, P12008 (2011).
- [33] T. Prosen, *New Journal of Physics* **10**, 043026 (2008).
- [34] J. Šuntajs, J. Bonča, T. Prosen, and L. Vidmar, arXiv preprint arXiv:1905.06345 (2019).
- [35] D. A. Abanin, J. H. Bardarson, G. De Tomasi, S. Gopalakrishnan, V. Khemani, S. A. Parameswaran, F. Pollmann, A. C. Potter, M. Serbyn, and R. Vasseur, arXiv preprint arXiv:1911.04501 (2019).
- [36] R. K. Panda, A. Scardicchio, M. Schulz, S. R. Taylor, and M. Žnidarič, *EPL* **128**, 67003 (2020).
- [37] L. Gordon, M. F. Schilling, and M. S. Waterman, *Probability Theory and Related Fields* **72**, 279 (1986).
- [38] D. Thouless, *Physics Reports* **13**, 93 (1974).
- [39] F. M. Izrailev, S. Ruffo, and L. Tessieri, *Journal of Physics A: Mathematical and General* **31**, 5263 (1998).
- [40] F. Pietracaprina, V. Ros, and A. Scardicchio, *Phys. Rev. B* **93**, 054201 (2016).
- [41] P. A. Lee and T. Ramakrishnan, *Reviews of Modern Physics* **57**, 287 (1985).
- [42] Z. Lenarčič, E. Altman, and A. Rosch, *Phys. Rev. Lett.* **121**, 267603 (2018).
- [43] Z. Lenarčič, O. Alberton, A. Rosch, and E. Altman, arXiv preprint arXiv:1910.01548 (2019).
- [44] V. Khemani, S. P. Lim, D. N. Sheng, and D. A. Huse, *Phys. Rev. X* **7**, 021013 (2017).
- [45] P. T. Dumitrescu, A. Goremykina, S. A. Parameswaran, M. Serbyn, and R. Vasseur, *Phys. Rev. B* **99**, 094205 (2019).

- [46] A. Goremykina, R. Vasseur, and M. Serbyn, *Phys. Rev. Lett.* **122**, 040601 (2019).
 [47] A. Morningstar, D. A. Huse, and J. Z. Imbrie, arXiv preprint arXiv:2006.04825 (2020).
 [48] T. Thiery, M. Müller, and W. De Roeck, arXiv preprint arXiv:1711.09880 (2017).
 [49] N. Laflorencie, G. Lemarié, and N. Macé, arXiv preprint arXiv:2004.02861 (2020).

A. Finding the NESS current

The NESS current corresponding to the system described by equations (1)-(4) can be calculated exactly, and here we briefly outline the method to do so. Detailed discussions and derivations of these equations can be found in Refs. 28, 29, and 33. We use the correlation matrix in the NESS to calculate the quantities of interest, namely the expectation values of the onsite magnetization σ_n^z and the current through the bond leaving site n in the positive direction $j_n = 2(\sigma_n^x \sigma_{n+1}^y - \sigma_n^y \sigma_{n+1}^x)$ (which can be derived from the continuity equation for the local magnetization). The correlation matrix is an $L \times L$ matrix from which we can calculate our quantities of interest: $\langle \sigma_n^z \rangle = -C_{n,n}$ and $\langle j_n \rangle = 4\Im(C_{n,n+1})$, where the NESS current j_∞ should be independent of n .

The correlation matrix is found by numerically solving the matrix equation

$$AC + CA^\dagger + G\tilde{C} + \tilde{C}G = P, \quad (\text{A1})$$

where \tilde{C} is the correlation matrix with the diagonal elements removed (note that for uniform dephasing, $\gamma_n = \gamma$, this reduces to equation 11 of Ref. 29). The non-Hermitian matrix $A = iE - iJ + \Gamma R$, where $E_{n,n} = h_n$, $J_{n,n\pm 1} = -1$ (note that $E - J$ is the Hamiltonian (1) in the single-particle sector), and $R_{1,1} = R_{L,L} = 1$. The remaining matrices are: $-P_{1,1} = P_{L,L} = 2\Gamma$ and $G_{n,n} = \gamma_n$. All unspecified matrix elements are zero.

When the disorder is strong and the system is large, the current j_∞ becomes small and imperfect numerical precision can result in the solution of (A1) being unphysical. This is easily diagnosed by studying the properties of the solution, such as the spatial invariance of the current, and whether the magnetization profile is real and bounded by $-1 \leq \langle \sigma_n^z \rangle \leq 1$. An alternative method of solving (A1) was presented in Ref. 30 for a system without dephasing, which can be gener-

alized to a system where $\gamma \neq 0$. Defining the non-Hermitian matrix $T = A + G$, we numerically find its complex eigenvalues λ_n and left and right eigenvectors $|\psi^{(Ri)}\rangle = \sum_k \psi_k^{(Ri)} |k\rangle$ and $|\psi^{(Li)}\rangle = \sum_k \psi_k^{(Li)} |k\rangle$, normalized such that $\langle \psi^{(Lm)} | \psi^{(Rn)} \rangle = \delta_{m,n}$. The eigenvectors are complex conjugates of each other $\psi_k^{(Li)} = (\psi_k^{(Ri)})^*$. We can rewrite (A1) as:

$$TC + CT^\dagger = \tilde{P}, \quad (\text{A2})$$

where \tilde{P} is a diagonal matrix with elements equal to $\tilde{P}_{n,n} = P_{n,n} + 2\gamma_n C_{n,n}$, which has the formal solution:

$$C = \int_0^\infty dt e^{-tT} \tilde{P} e^{-tT^\dagger}. \quad (\text{A3})$$

Rewriting this in the eigenbasis of T and evaluating the integral we find a set of equations:

$$C_{m,n} = \Gamma(\theta_{m,n,1} - \theta_{m,n,L}) + \sum_k \gamma_k \theta_{m,n,k} C_{k,k}, \quad (\text{A4})$$

where we have introduced the shorthand:

$$\theta_{j,k,l} = 2 \sum_{p,q} \frac{\psi_j^{(Rp)} \psi_l^{(Rp)} (\psi_k^{(Rq)} \psi_l^{(Rq)})^*}{\lambda_p + \lambda_q^*}. \quad (\text{A5})$$

After numerically diagonalizing the matrix T the quantities $\theta_{j,k,l}$ can be constructed easily. The diagonal elements, which describe the magnetization profile $\langle \sigma_n^z \rangle = -C_{n,n}$, give us a set of L linear equations:

$$\langle \sigma_n^z \rangle = \Gamma(\theta_{n,n,1} - \theta_{n,n,L}) + \sum_m \gamma_m \theta_{n,n,m} \langle \sigma_m^z \rangle, \quad (\text{A6})$$

which can be solved numerically. With the knowledge of the diagonal elements we can then simply evaluate the currents:

$$\langle j_n \rangle = 4\Im \left(\Gamma [\theta_{n,n+1,L} - \theta_{n,n+1,1}] - \sum_m \gamma_m \theta_{n,n+1,m} \langle \sigma_m^z \rangle \right). \quad (\text{A7})$$

Note that in order to calculate the magnetization profile and the current through every bond it is not necessary to evaluate all L^3 of the $\theta_{j,k,l}$ quantities.